

## Article

# One-Step Synthesis of High-Performance N/S Co-Doped Porous Carbon Material for Environmental Remediation

Xiaoyu Huo<sup>1,2</sup>, Chao Jia<sup>2</sup>, Shanshan Shi<sup>1,2</sup>, Tao Teng<sup>2</sup>, Shaojie Zhou<sup>2</sup>, Mingda Hua<sup>2</sup>, Xiangdong Zhu<sup>2,3</sup>, Shicheng Zhang<sup>1,2,\*</sup>  and Qunjie Xu<sup>1,\*</sup>

- <sup>1</sup> College of Environmental and Chemical Engineering, Shanghai University of Electric Power, Shanghai 200090, China; huoxiaoyu@mail.shiep.edu.cn (X.H.); shanshanshi@mail.shiep.edu.cn (S.S.)
- <sup>2</sup> Shanghai Technical Service Platform for Pollution Control and Resource Utilization of Organic Wastes, Shanghai Key Laboratory of Atmospheric Particle Pollution and Prevention (LAP3), Department of Environmental Science and Engineering, Fudan University, Shanghai 200438, China; 20110740026@fudan.edu.cn (C.J.); 20210740076@fudan.edu.cn (T.T.); sjzhou17@fudan.edu.cn (S.Z.); 20210740045@fudan.edu.cn (M.H.); zxdjewett@fudan.edu.cn (X.Z.)
- <sup>3</sup> Shanghai Institute of Pollution Control and Ecological Security, Shanghai 200092, China
- \* Correspondence: zhangsc@fudan.edu.cn (S.Z.); xuqunjie@shiep.edu.cn (Q.X.)

**Abstract:** Potassium thiocyanate (KSCN), a highly efficient “three birds with one stone” activator, might work with inorganic activators to produce excellent N/S co-doped porous carbon (NSC) materials for environmental remediation. However, the effects of inorganic activators on cooperative activation are unclear. As a result, the influence of inorganic activators on the synthesis of NSC materials was investigated further. This study shows that the surface areas of the NSC materials acquired through cooperative activation by potassium salts (KOH or K<sub>2</sub>CO<sub>3</sub>) were considerably higher than those acquired through KSCN activation alone (1403 m<sup>2</sup>/g). Furthermore, KSCN could cooperate with K<sub>2</sub>CO<sub>3</sub> to prepare samples with excellent specific surface area (2900 m<sup>2</sup>/g) or N/S content. The as-prepared NSC materials demonstrated higher adsorption capability for chloramphenicol (833 mg/g) and Pb<sup>2+</sup> (303 mg/g) (pore fitting, complexation). The research provides critical insights into the one-step synthesis of NSC materials with a vast application potential.

**Keywords:** N/S co-doping; porous carbon; chloramphenicol adsorption; Pb<sup>2+</sup> removal



**Citation:** Huo, X.; Jia, C.; Shi, S.; Teng, T.; Zhou, S.; Hua, M.; Zhu, X.; Zhang, S.; Xu, Q. One-Step Synthesis of High-Performance N/S Co-Doped Porous Carbon Material for Environmental Remediation.

*Processes* **2022**, *10*, 1359. <https://doi.org/10.3390/pr10071359>

Academic Editor: Avelino Núñez-Delgado

Received: 12 June 2022

Accepted: 11 July 2022

Published: 12 July 2022

**Publisher's Note:** MDPI stays neutral with regard to jurisdictional claims in published maps and institutional affiliations.



**Copyright:** © 2022 by the authors. Licensee MDPI, Basel, Switzerland. This article is an open access article distributed under the terms and conditions of the Creative Commons Attribution (CC BY) license (<https://creativecommons.org/licenses/by/4.0/>).

## 1. Introduction

Because of the ongoing energy crisis and environmental concerns, the production and application of carbon materials derived from biomass has recently garnered a lot of interest [1–7]. As biomass resources are abundant and sustainable in the environment, they are considered as renewable carbon precursors of porous carbon materials [8]. The incorporation of heteroatoms into carbon frameworks enriches the surface functional groups and improves the chemical properties of materials' surfaces [9–11]. For example, the introduction of N elements could improve the surface polarity of carbon materials, thus improving the hydrophilicity and number of reactive sites on the materials [12–14]. Other studies have suggested that S heteroatoms could boost the chemical reactivity of carbon materials and greatly improve their affinity to heavy metals [15,16]. Benefiting from the synergistic effects of different heteroatoms, co-doping with multiple heteroatoms improves the overall performance of porous carbon materials more effectively than single-atom doping [17]. Therefore, much effort has been expended on the synthesis of heteroatom-doped porous carbon materials from biomass.

Currently, the most basic ways for creating heteroatom-doped porous carbon materials derived from biomass are self-doped technologies, which require the use of inorganic activators (such as KOH and ZnCl<sub>2</sub>) to directly activate the biomass-containing heteroatom sources (e.g., N, S, or P sources) [18–20]. The performance of the resulting heteroatom-doped carbon materials critically depends on the reaction of the inorganic activators with

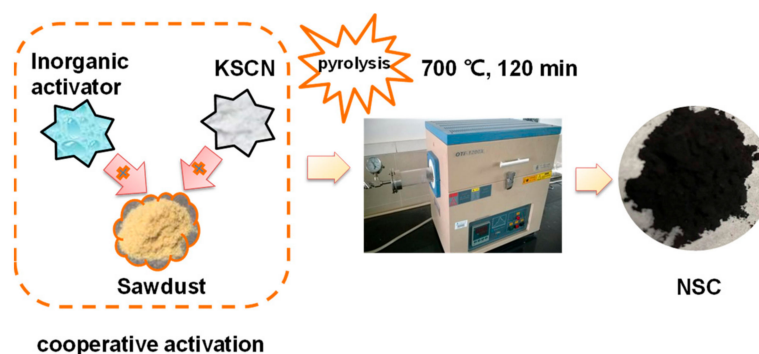
the heteroatoms in the biomass during the activation process. However, as self-doping technology relies on the heteroatom concentration of the biomass precursor, this limits its applicability range. As a result, most techniques have concentrated on mixing inorganic activators (e.g., KOH, K<sub>2</sub>CO<sub>3</sub>, or CaCl<sub>2</sub>) with organic dopants (e.g., urea, melamine, or thiourea), which cooperatively activate biomass to synthesize heteroatom-doped porous carbon materials [21–25]. It has been shown, for example, that K<sub>2</sub>CO<sub>3</sub> and urea could be utilized as a cooperative activator to prepare N-doped porous carbon materials with a large surface area from biomass [26]. Through the complexation of inorganic activators and N-dopants, an N-containing metal oxide (e.g., KOCN) could be formed through this synthetic method, and the porosity of the samples would be improved by the subsequent carbothermal reduction reaction (KOCN + C → KCN + CO) [27]. However, the simultaneous activation of inorganic activators and organic dopants is both resource consuming and difficult, requiring excess dopants to obtain a satisfactory heteroatom-doped carbon material. In recent research, we discovered that KSCN, a “three birds with one stone” activator plays dual roles of porogen and dopant. More specifically, KSCN achieves simultaneous pore generation and N/S doping through an oxygen displacement reaction [28]. KSCN is far superior to standard organic dopants owing to its high heteroatom doping capability and minimal carbon content. Meanwhile, KSCN might also work with inorganic activators to improve the material characteristics via the carbothermal reduction process. However, the synergistic activation of biomass by inorganic activators and KSCN has been little explored in the preparation of carbon materials.

To address this need, the present study examines the impacts of several inorganic activators (KOH, K<sub>2</sub>CO<sub>3</sub>, and ZnCl<sub>2</sub>) on the characteristics (porosity and N/S content) of NSC materials. Simultaneously, the influence of K<sub>2</sub>CO<sub>3</sub> and KSCN loading contents on the porosity and N/S doping of materials was explored further. Furthermore, the potential of NSC materials to treat water was thoroughly investigated.

## 2. Materials and Methods

### 2.1. Synthesis of NSC Materials

Sawdust was obtained from rural Shanghai. Other reagents were purchased from Shanghai Aladdin Biochemical Technology Co., Ltd (Shanghai, China). The samples were synthesized as shown in Scheme 1. The NSC material was prepared by activation of sawdust (80 mesh) and mixed with inorganic activators and potassium thiocyanate (KSCN, AR = 98.5%). Then the mixture was shaken in an aqueous solution for the period of 12 h and dried at 80 °C in air for 12 h before heating to 700 °C for 2 h at a heating rate of 10 °C min<sup>-1</sup> in a tube furnace. The N<sub>2</sub> gas flow was controlled at 100 mL min<sup>-1</sup>. Various inorganic activators, including K<sub>2</sub>CO<sub>3</sub> (AR = 99%), KOH (AR = 85%), and ZnCl<sub>2</sub> (AR = 98%), were used to prepare NSC material at 700 °C with an inorganic activator/KSCN/biomass weight ratio of 1:1:1. Then, the effects of loading contents of K<sub>2</sub>CO<sub>3</sub> and KSCN on the porosity and doping of N/S in materials were further investigated. For this purpose, the activator-to-biomass mass ratio was adjusted to be 0, 1, 1/2, and 1, respectively. The carbonized samples were further washed with 2 M HCl to completely remove any salt residues, and were then washed repeatedly with deionized water before oven-drying at 100 °C until constant weight.



**Scheme 1.** Schematic of the NSC synthesis.

## 2.2. Characterizations of Materials

The elemental analyzer (Vario EL III) was used to perform elemental composition (C, H, N, S) analysis. The ash contents from materials were analyzed after heating materials in the air at 600 °C for 2 h. Using a Quantachrome Autosorb iQ2 apparatus, N<sub>2</sub> adsorption/desorption isotherms (at 77 K) was conducted to measure surface areas and pore volumes. Materials were further degassed at 120 °C for the period of 12 h before any further analysis. In this study, the Brunauer–Emmett–Teller (BET) equations were used to calculate surface areas ( $S_{\text{BET}}$ ) and total pore volumes ( $V_{\text{T}}$ ). Surface areas of micropores ( $S_{\text{mic}}$ , < 2 nm) were then determined via the t-plot analysis. The distribution of pore sizes was estimated using theoretical model such as density functional theory (DFT) [27]. The crystal structures of pristine samples were performed using powder X-ray diffractometry (XRD, X'Pert PRO), which was provided with Cu K $\alpha$  radiation (40 mA, 40 kV). The  $2\theta$  range was performed from 10 to 80°. Raman spectra were further obtained by a Raman spectrometer (XploRA) with a laser of 532 nm. Five Gaussian peaks G, D, I, D', and D'' at  $\sim 1580$ ,  $\sim 1350$ ,  $\sim 1220$ ,  $\sim 1620$ , and D''  $\sim 1490$  cm<sup>-1</sup>, were fitted by parameters. The surface functionality of NSC materials containing N- and S- were measured using X-ray photoelectron spectroscopy (XPS, Thermo ESCALAB 250 XI). The N 1s spectra peaks of pyridinic, pyrrolic, quaternary, and oxidized nitrogen were fitted by deconvolution. Additionally, S<sub>2p</sub> spectra included the bonding of C–SO<sub>3</sub>, C–SO<sub>2</sub>, C–S–C 2p<sub>1/2</sub>, and C–S–C 2p<sub>3/2</sub>. Binding energies were calibrated using the C 1s with the value of 284.6 eV. The peak data were fitted using XPS peak41 software. The morphology of the material was examined using scanning electron microscope (SEM, NovaNanoSem 450, FEI). The released CO gas at  $\sim 700$  °C (peak 3) during cooperative activation by inorganic activator and KSCN was determined using mass spectrometer (Hiden QIC-20, MS). The m/z value for CO was set for 28.

## 2.3. Adsorption Experiments

The typical organic pollutant chloramphenicol (CAP) was chosen to evaluate the ability to purify water for NSC materials [29]. For the adsorption kinetic, 2.5 mg material was added to 25 mL of 120 mg/L CAP solution, and then 2 mL of the solution was collected at 2, 5, 10, 30, and 60 min for CAP concentration analysis. Batch experiments for adsorption were carried out as follows: material with 2.5 mg was dispersed in 25 mL of CAP solutions at different concentration (5–120 mg/L). The mixture was continuously shaken at the speed of 150 rpm for 12 h at 25 °C. After reaching adsorption equilibria, the supernatants were then filtered by an organic membrane with the pore size of 0.22  $\mu\text{m}$  to analyze CAP concentrations. The contents of CAP were determined using an Agilent 1260 liquid chromatography, which was equipped with a C18 column at 25 °C and an ultraviolet detector at 278 nm wavelength, and the mobile phase was 6:4 (v/v) of the mixture of ultrapure water and methanol.

The toxic heavy metals such as lead(II) (Pb<sup>2+</sup>) have attracted extensive attention for causing serious problems to the ecological environment and human health; thus, Pb<sup>2+</sup> adsorption ability by the N/S co-doped carbon material was further evaluated [30]. For lead(II) (Pb<sup>2+</sup>) adsorption isotherm, material with 20 mg was dispersed in 40 mL of Pb<sup>2+</sup>

solutions, which have various concentrations ranging from 20 to 600 mg/L. Furthermore, 10 mM MES solutions were added to stabilize the pH of the solution. The mixture was constantly shaken at 150 rpm for the period of 12 h. After adsorption equilibrium, the concentration of  $\text{Pb}^{2+}$  was measured using ICP-AES (Hitachi P4010). A transmission electron microscopy (TEM-TecnaiG2F20 S-Twin FEI) was employed to explore the adsorption mechanism for NSC material. Langmuir model was used for data fitting of adsorption isotherms, and the model of pseudo-second-order was applied to interpret the adsorption mechanism, which was explicated in our previous work [31,32].

### 3. Results and Discussions

#### 3.1. Effect of Inorganic Activator Type on the NSC Materials' Properties

The effect of inorganic activator types on the properties of NSC materials was investigated first. As shown in Table 1, compared with the NSC materials acquired through KSCN activation only, the surface areas of the NSC materials achieved by means of potassium salts' (KOH or  $\text{K}_2\text{CO}_3$ ) cooperative activation were significantly increased. At the same time, the pore size distribution showed that the degree of porosity with the sizes less than 2 nm increased significantly, and, particularly, the supermicropore ( $0.7 \text{ nm} < \text{pore size} < 2 \text{ nm}$ ) was increased (Figure 1a). These results indicated that potassium salts (KOH or  $\text{K}_2\text{CO}_3$ ) had strong cooperative activation abilities. The KCN signals in the XRD spectra (Figure 1b) established that carbothermal reduction reactions ( $\text{KOCN} + \text{C} \rightarrow \text{KCN} + \text{CO}$ ) occurred during the cooperative activation by potassium salts (KOH or  $\text{K}_2\text{CO}_3$ ) and KSCN, which was a widely known pore-forming reaction [33]. Moreover, the high yield for CO gas at peak 3 (greater than  $700 \text{ }^\circ\text{C}$ ) further proved the previous assumption (Figure S1a). Furthermore, it was also worth explaining that the release of CO at the low temperatures (peaks 1 and 2) were found to result from the biomass pyrolysis. However, the excessive CO generated with the carbothermal reduction could result in the enlarging of micropores. As shown in Table 1, the microporosity of KOH-derived NSC material was obviously lower than that of  $\text{K}_2\text{CO}_3$ -derived NSC material.

**Table 1.** NSC elemental compositions and textural characteristics of NSC produced with various types of inorganic activators. The activation conditions were set to be  $700 \text{ }^\circ\text{C}$ , inorganic activator: KSCN: biomass mass ratio = 1:1:1.

Inorganic Activator	Yield (%)	Ash (%)	C (%)	N (%)	S (%)	$S_{\text{BET}}^a$ ( $\text{m}^2/\text{g}$ )	$S_{\text{mic}}^b$ ( $\text{m}^2/\text{g}$ )	$V_{\text{T}}^c$ ( $\text{cm}^3/\text{g}$ )	$V_{\text{super}}^d$ ( $\text{cm}^3/\text{g}$ )	$V_{\text{ultra}}^e$ ( $\text{cm}^3/\text{g}$ )
/	38.7	5.65	65.7	5.03	10.01	1403	1040 (74)	1.17	0.29	0.18
$\text{K}_2\text{CO}_3$	26.3	4.67	71.44	2.98	9.75	2397	1970 (82)	1.24	0.63	0.13
KOH	21.2	6.05	79.35	2.28	5.67	2439	1568 (64)	1.38	0.59	0.14
$\text{ZnCl}_2$	93.9	38	38	4.46	18.09	129	- <sup>f</sup>	0.29	0.01	-

<sup>a</sup> BET surface area; <sup>b</sup> micropore surface area, the values in parenthesis are the  $S_{\text{mic}}/S_{\text{BET}}$  and the unit is %; <sup>c</sup> total pore volume; <sup>d</sup> supermicropore volume ( $0.7 \text{ nm} < \text{pore size} < 2 \text{ nm}$ ); <sup>e</sup> ultramicropore volume ( $< 0.7 \text{ nm}$ ); and <sup>f</sup> not detected.

It is worth noting that the BET results showing the surface area of the carbon sample achieved by  $\text{ZnCl}_2$  cooperative activation was only  $129 \text{ m}^2/\text{g}$  (Table 1), indicating that the cooperative activation ability of  $\text{ZnCl}_2$  was relatively low. Therefore, it was inferred that the formation of ZnS hinders the carbothermal reduction reaction. The obvious ZnS signals presented in the material obtained by  $\text{ZnCl}_2$  cooperative activation further proved the above results (Figure 1b). Furthermore, compared with the NSC material obtained by the individual activation of KSCN, the N contents of the NSC samples prepared by cooperative activation of potassium salts (KOH or  $\text{K}_2\text{CO}_3$ ) significantly decreased (Table 1). Therefore, it was concluded that the carbothermal reduction reaction occurs with a decrease in nitrogen content [28]. The results were further confirmed by the lower N content in the NSC materials obtained by the excessive cooperative activation of KOH than in the materials

derived from  $K_2CO_3$ . Therefore, the inorganic activators were essential for the one-step synthetic pathway for N/S co-doping into carbon materials with excellent properties.

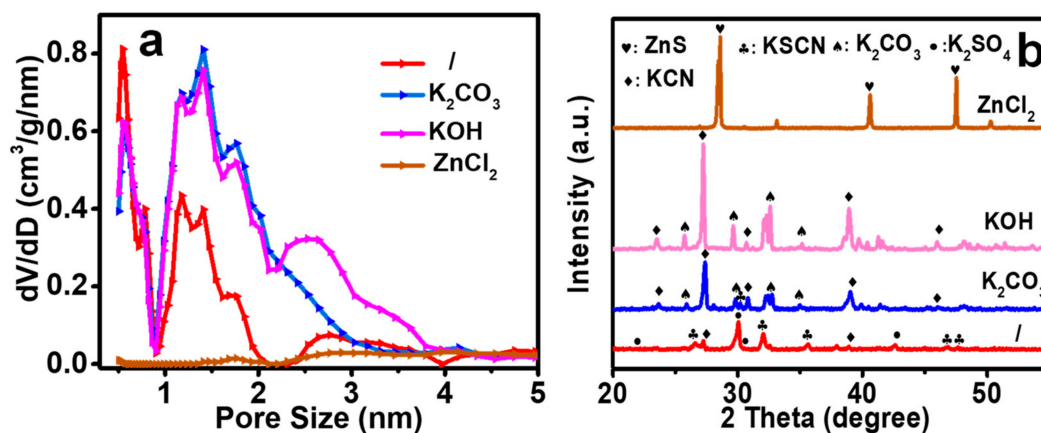


**Figure 1.** (a) The distribution of pore sizes for NSC, which were produced by being thermally induced using different inorganic activator, (b) XRD patterns for the unwashed NSC produced by being thermally induced using different inorganic activator. The activation conditions were set to be 700 °C, and the mass ratio of inorganic activator: KSCN: biomass was 1:1:1.

### 3.2. Effect of $K_2CO_3$ Load Content on the NSC Materials' Properties

The effects of the load content of  $K_2CO_3$  on the pore structure and N/S doping into synthetic NSC materials were also examined. The SEM images showed that the surface of the NSC sample derived by the self-induction of KSCN was found to be less porous (Figure 2a), whereas the NSC material obtained from  $K_2CO_3$  cooperative activation had great crosslinked pores (Figure 2b). This result indicated that  $K_2CO_3$  cooperative activation could improve the pore structure of NSC materials. As demonstrated in Figure S2b, the singles of  $K_2SO_4$  in the XRD spectra of the KSCN-derived NSC materials were attributed to the oxygen displacement reaction between the biomass and KSCN, which could effectively generate pores and achieve co-doping of N/S [28]. With the increasing load content of  $K_2CO_3$ , the KCN signals gradually strengthened (Figure S2b), while the yield significantly decreased as shown in Table S1. The data imply a gradually enhancing carbothermal reduction reaction ( $KOCN + C \rightarrow KCN + CO$ ), which was further confirmed by the increasing CO gas (peak 3 in Figure 2c). At the same time, the isotherms of  $N_2$  adsorption (type I(b)) for the NSC materials further confirmed that high microporosity of the NSC materials could be achieved by the cooperative activation of  $K_2CO_3$  (Figure S2a) [34]. The pore size distributions (Figure 2d) were concentrated in two regions: 0.5–0.7 nm and 1.1–2.0 nm. Furthermore, with the increasing load content of  $K_2CO_3$ , the pores accompanying with sizes less than 2 nm obviously increased ( $V_{super}$  reached 0.68 when  $K_2CO_3$  ratio was found to be 2), thereby boosting the BET surface area of the NSC samples to 2900  $m^2/g$  for the NSC samples (Table S1), outperforming the previously reported N/S-doped carbon materials [8].

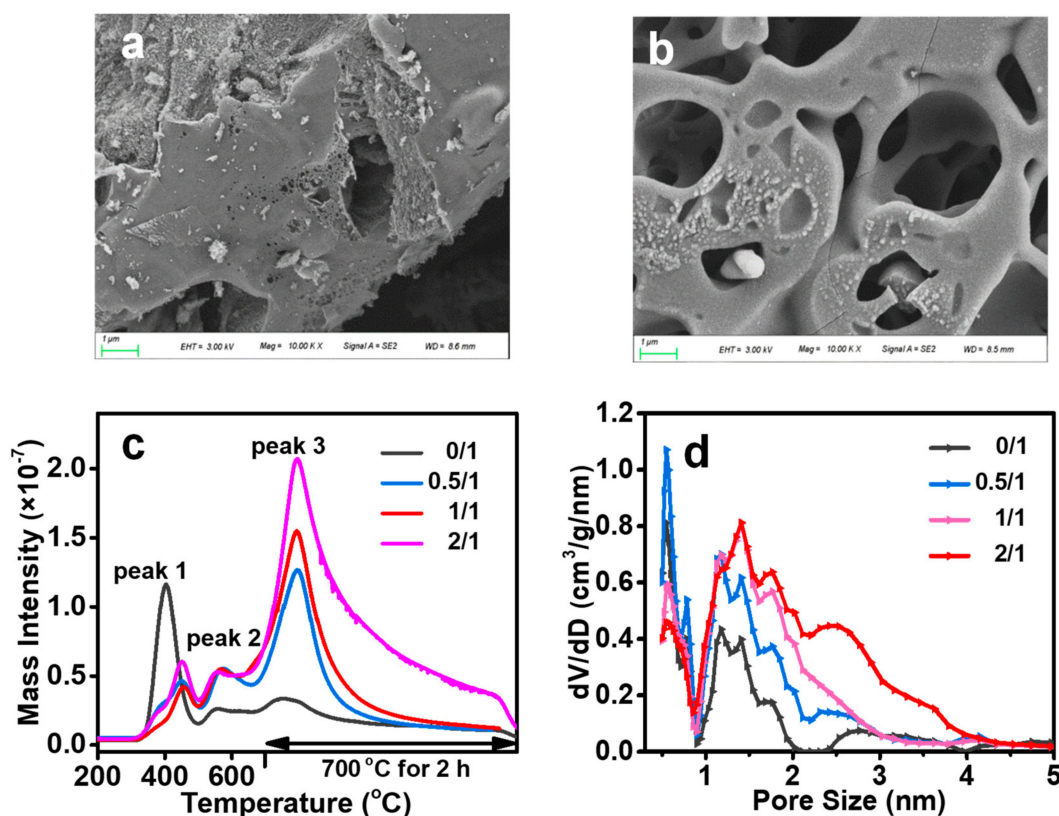


**Figure 2.** (a) Typical SEM images of NSC prepared by thermal activation of KSCN, (b) SEM images of NSC prepared by thermal activation of K<sub>2</sub>CO<sub>3</sub> and KSCN, (c) the CO release graphs and (d) distribution of pore sizes of NSC, which were activated with various loading contents of K<sub>2</sub>CO<sub>3</sub>. The activation conditions were set to be 700 °C, KSCN: biomass mass ratio = 1:1, K<sub>2</sub>CO<sub>3</sub>: KSCN: biomass mass ratio = 2:1:1.

As shown in Table S1, the N contents of the NSC materials gradually reduced with the expanding loading content of K<sub>2</sub>CO<sub>3</sub>. This result also strongly indicated that the reaction of carbothermal reduction normally sacrifices some of the nitrogen content [27,35]. Four peaks were observed in the NSC samples by deconvolution of the N 1s spectrum, consisting of pyridine, pyrrole, quaternary, and oxide of nitrogen (Figure 3a). As shown in Figures 3a and S3a, the decrease in the amount of pyridinic nitrogen in the N 1s XPS spectra suggested a favorable role of this nitrogen form in the joint reactions between K<sub>2</sub>CO<sub>3</sub> and KSCN. It is also noteworthy that the S content of the NSC materials remained stable with the increasing loading content of K<sub>2</sub>CO<sub>3</sub> (weight ratio of K<sub>2</sub>CO<sub>3</sub> and biomass < 1), inferring that S did not participate in the above reaction (Table S1). The established C-SO<sub>2</sub> and C-SO<sub>3</sub> peaks in the spectra of S 2p further confirmed the inference (Figure 3b). However, excessive K<sub>2</sub>CO<sub>3</sub> activators (weight ratio of K<sub>2</sub>CO<sub>3</sub> and biomass > 1), led to a considerable reduction in the S contents in the NSC materials (Table S1). Raman spectra showed that K<sub>2</sub>CO<sub>3</sub> activation could also enhance the graphitization degree of the NSC materials, which was confirmed by the decreased  $I_D/I_G$  value (Figure S3b). In summary, the addition of inorganic activators in the one-step synthesis process of NSC materials definitively affected the structure of pores and N/S doping.

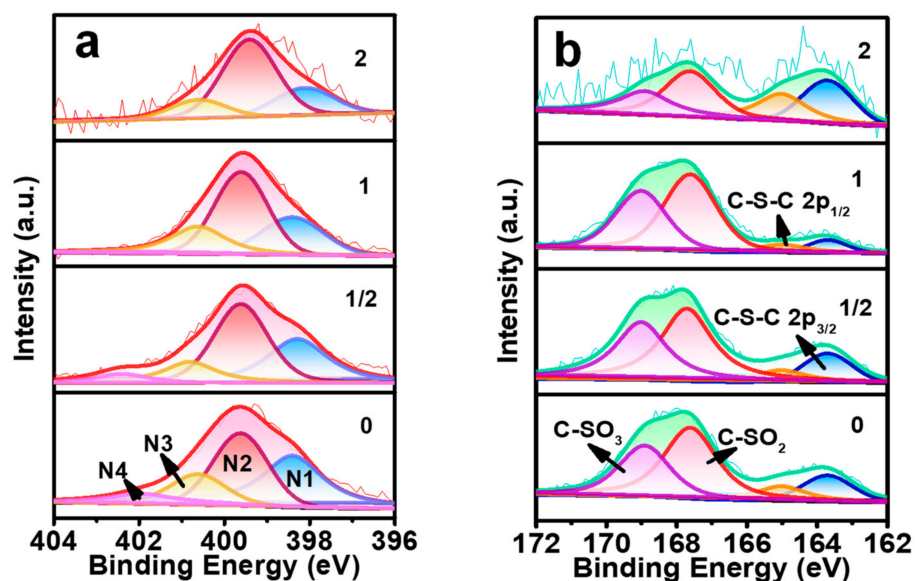


**Figure 3.** (a) N1s XPS spectra for different  $K_2CO_3$  loading content-induced NSC materials (N1 pyridinic N, N2 pyrrolic N, N3 quaternary N, N4 oxidic N), (b) S 2p spectra for different  $K_2CO_3$  loading content-initiated NSC materials. The activation conditions were set to be 700 °C, KSCN: biomass mass ratio = 1:1, various mass ratios between  $K_2CO_3$  and biomass.

### 3.3. Effect of KSCN Load Content on the NSC Materials' Properties

The BET surface areas of the NSC materials achieved by collaborative initiations were significantly enhanced, and this enhancement was much more extensive than those of the porous carbon (PC) materials obtained by  $K_2CO_3$  activation (Table S2). This result indicates that the KSCN was highly involved in the activation of biomass. When the mass ratio between KSCN and biomass grew to 1, the yields for NSC reduced but the BET surface area for the NSC improved (Table S2). The distribution curves of pore size showed that the number of pores with a size smaller than 2 nm increased (Figure 4a). These results imply that KSCN played an important role in instigating the reduction reactions ( $KOCN + C \rightarrow KCN + CO$ ), as further proved by the steadily raised KCN intensity in the XRD spectra of pristine NSC samples (Figure 4b). Meanwhile, the CO gas production (peak 3) increased with the increasing loading content of KSCN, further confirming the above conclusions (Figure 4c). However, extra KSCN activators (weight ratio of KSCN and biomass > 1) led to the decline in the porosity in the NSC materials, which might be attributed to the pore cracking caused by excessive cooperative activation. The  $V_{super}$  and  $V_{ultra}$  also showed the same trend (Table S2). Simultaneously, the yield of NSC was significantly improved with the increasing loading content of KSCN (weight ratio of KSCN and sawdust > 1, Table S2); thus, it could be concluded that the excess KSCN could also serve as a carbon source in initiating the carbothermal reduction for biomass. Interestingly, the deconvolution results of S in NSC proved that O could mix with sulfur to produce sulfur–oxygen bonding such as C-SO<sub>2</sub> and C-SO<sub>3</sub> (Figure S4a). The oxygen content was raised when the S content was enhanced in NSC, which complied well with the above conclusion (Table S2). In addition, the raised N/S content resulted in the slight decrease in the graphitization degree of NSC (indicated by the increased  $I_D/I_G$  value) (Figure S4b).

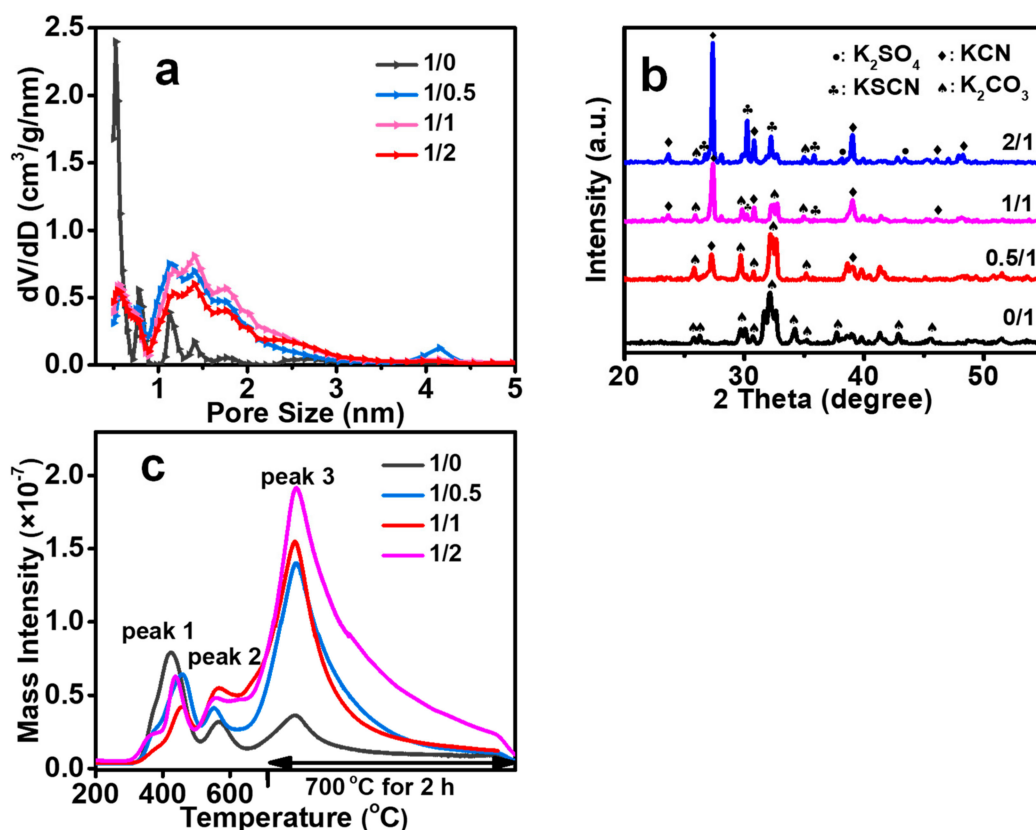


**Figure 4.** (a) Pore size in NSC materials, (b) XRD patterns of the unwashed NSC materials, (c) CO release curves of the NSC materials. The activation conditions were set to be 700 °C,  $K_2CO_3$ : biomass mass ratio of = 1:1, various mass ratios between KSCN and biomass.

### 3.4. The NSC Materials for Water Purification

The water purification performance of the NSC materials with different specific surface areas and N/S amounts was evaluated. The samples were labeled with A-x, in which x denotes various sample types (Table S3). As displayed in Figure 5a and Table S4, the NSC materials showed a higher adsorption capacity of CAP (maximum 833 mg/g) than that of previously reported materials [36–38]. The results of adsorption kinetics indicated that the adsorption equilibrium was reached at 30 min, which could be explained by the developed microporous structure of NSC (Figure S5a). Furthermore, the parameters for pseudo-second-order kinetic models were fitted to further reveal the adsorption process (Table S4). The adsorption capacity of CAP increased with the growing BET surface area of the NSC materials (Figure S5b,c), indicating that the pore-fitting mechanism might be essential for adsorption property. In addition, the CAP adsorption capacity for the per surface area ( $CAP-q_{BET}$ ) of the NSC materials was further analyzed. The  $CAP-q_{BET}$  of the NSC materials was higher than the PC materials, suggesting that N doping played a positive role in CAP adsorption (Figure 5b).

$Pb^{2+}$  containing wastewater poses extensive risks to the ecological environment and human health. The Langmuir model was used for fitting adsorption isotherms. The maximum adsorption capacities for  $Pb^{2+}$  varied from 100 mg/g to 303 mg/g (Figure S6a and Table S5). The significant difference in the adsorption of  $Pb^{2+}$  might be explained by changes in the sulfur contents of the NSC materials, and the results were confirmed using the positive correlation between the sulfur contents and maximum adsorption capacity ( $R^2 = 0.96$ ) (Figure 6a). Therefore, the material exhibits an excellent adsorption capacity for  $Pb^{2+}$  in water. Furthermore, it was discovered that there were consistent fluctuations in the distribution and mass transfer for sulfur and Pb in TEM-EDS (Figure 6b). These observations proved that the  $Pb^{2+}$  could be fixed by complexing with the S-containing

functional groups present in NSC samples. The excellent adsorption ability of materials for  $Pb^{2+}$  might be attributed to the complexation of S-containing functional groups on NSC materials.

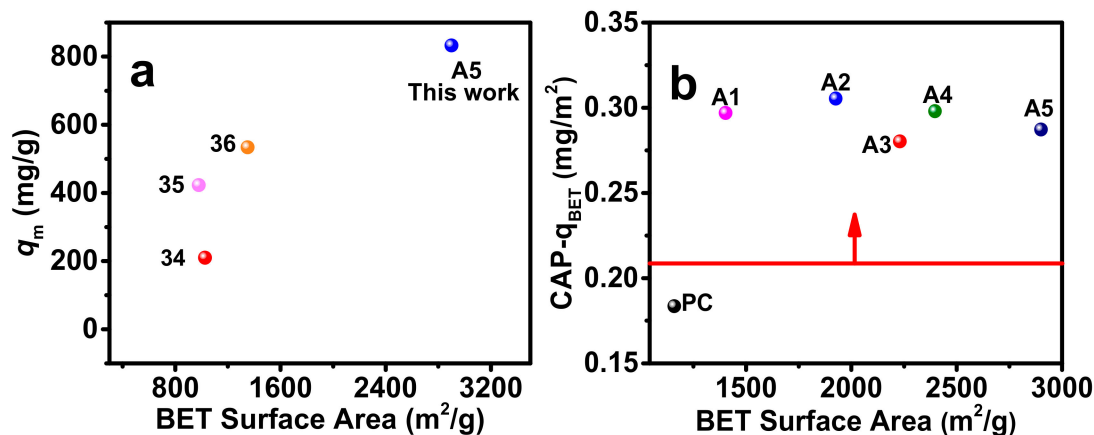


**Figure 5.** (a) Adsorption capacity ( $q_m$ ) of CAP versus BET surface area, plotted for previously reported materials and the materials prepared in this study, (b) BET surface area of selected NSC material versus  $CAP-q_{BET}$ .  $q_{BET} = q_m/BET$  surface area, suggesting CAP adsorption capacity per BET surface area. PC: porous carbon material activated with  $K_2CO_3$ , activation temperature = 700 °C,  $K_2CO_3$ : biomass mass ratio = 1:1.

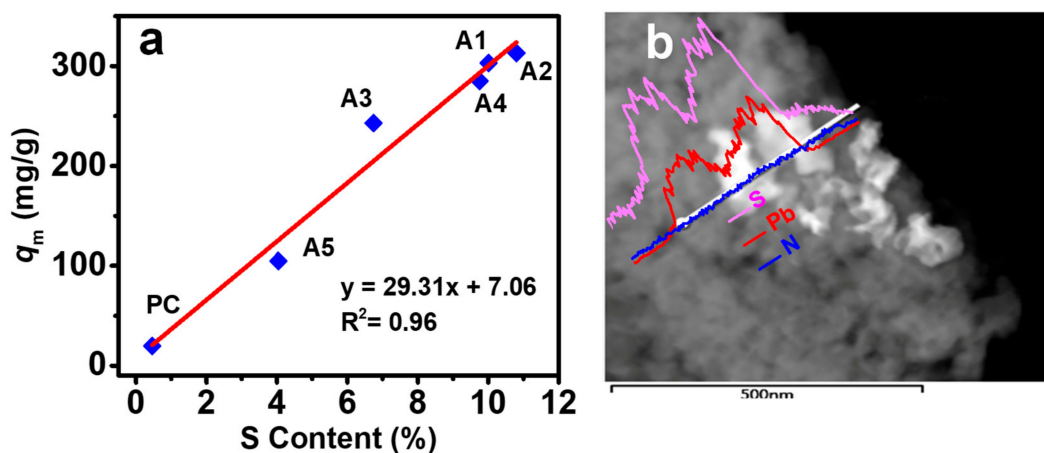


**Figure 6.** (a) Linear correlation between  $q_m$  and S content of NSC material, (b) representative TEM-EDS line profiles of elements in the selected NSC material (A1) after  $Pb^{2+}$  adsorption. PC: porous carbon material activated with  $K_2CO_3$ , activation temperature = 700 °C,  $K_2CO_3$ : biomass mass ratio = 1:1.

#### 4. Conclusions

In this study, the effect of the inorganic activators on the properties of NSC materials were investigated. This study suggested that potassium salt could significantly promote the NSC materials' properties due to the strong carbothermal reduction reaction. Furthermore, the porosity and doping of nitrogen and sulfur into the obtained materials could be effectively improved by adjusting the mass ratio of KSCN to  $K_2CO_3$ . The results indicated that the as-prepared material exhibited a larger BET surface area of 2900  $m^2/g$  or the high content of N/S. The NSC materials presented a high organic pollutant removal capacity (~833 mg/g CAP adsorption) owing to their porous properties. In addition, the doping of S greatly improved the ability of carbon materials to remove  $Pb^{2+}$  in wastewater due to the complexation effect. The results have substantial consequences for the controllable synthesis of NSC materials.

**Supplementary Materials:** The following supporting information can be downloaded at: <https://www.mdpi.com/article/10.3390/pr10071359/s1>, Figure S1. (a) Different inorganic activator on the release curves of CO during the preparation process of NSC materials. The activation conditions were set to be 700 °C, and inorganic activator, KSCN and biomass with weight ratio of 1:1:1. Figure S2. (a) N<sub>2</sub> adsorption–desorption isotherms of NSC materials, (b) XRD patterns of the unwashed NSC materials. The activation conditions were set to be 700 °C, KSCN and biomass with mass ratio of 1:1, various mass ratio between K<sub>2</sub>CO<sub>3</sub> and biomass. Figure S3. (a) Relative ratio of pyridinic N (N1) and pyrrolic N (N2) for NSC materials, (b) Raman spectrum of NSC materials was fitted using the five Gaussian peaks (color lines). The activation conditions were set to be 700 °C, KSCN and biomass with weight ratio of 1:1, various weight ratios between K<sub>2</sub>CO<sub>3</sub> and biomass. Figure S4. (a) S 2<sub>p</sub> XPS spectra for different KSCN loading content-induced NSC materials, (b) Raman spectrum of NSC materials was fitted using the five Gaussian peaks (color lines). The activation conditions were set to be 700 °C, K<sub>2</sub>CO<sub>3</sub> and biomass with weight ratio of 1:1, various weight ratios between KSCN and biomass. Figure S5. (a) Adsorption kinetics of CAP onto selected NSC, (b) correlations of the resultant NSC between maximum adsorption capacity ( $q_m$ ) and BET surface area, (c) adsorption isotherms of CAP for selected NSC in aqueous solution (the adsorption isotherms were fitted with the Langmuir model). Figure S6. (a) Adsorption isotherms of Pb<sup>2+</sup> for selected NSC in aqueous solution (the adsorption isotherms were fitted with the Langmuir model). Table S1. Elemental compositions and textural properties of NSC samples. The activation conditions were set to be 700 °C, KSCN and biomass with weight ratio of 1:1, various weight ratios between K<sub>2</sub>CO<sub>3</sub> and biomass. Table S2. Elemental compositions and textural properties of NSC samples. The activation conditions were set to be 700 °C, K<sub>2</sub>CO<sub>3</sub> and biomass with weight ratio of 1:1, various weight ratios between KSCN and biomass. Table S3. Porosity, preparation condition, and elemental compositions of selected NSC materials. The activation conditions were set to be 700 °C. Table S4. The isothermal parameters and kinetic parameters of selected NSC materials for CAP adsorption. Table S5. The isothermal parameters of selected NSC materials for Pb<sup>2+</sup> adsorption.

**Author Contributions:** Writing—Original draft, X.H.; methodology, C.J. and S.S.; data curation, T.T., S.Z. (Shaojie Zhou), M.H. and X.Z.; funding acquisition, S.Z. (Shicheng Zhang) and Q.X. All authors have read and agreed to the published version of the manuscript.

**Funding:** This research was supported by the National Natural Science Foundation of China (No. 21876030), the International Cooperation Project of Science and Technology Commission of Shanghai Municipality (No. 18230710700).

**Institutional Review Board Statement:** Not applicable.

**Informed Consent Statement:** Not applicable.

**Data Availability Statement:** Not applicable.

**Conflicts of Interest:** The authors declare no conflict of interest.

## References

1. Deng, J.; Li, M.M.; Wang, Y. Biomass-derived carbon: Synthesis and applications in energy storage and conversion. *Green Chem.* **2016**, *18*, 4824–4854. [[CrossRef](#)]
2. Fu, R.; Yu, C.; Li, S.F.; Yu, J.H.; Wang, Z.; Guo, W.; Xie, Y.Y.; Yang, L.; Liu, K.L.; Ren, W.C.; et al. A closed-loop and scalable process for the production of biomass-derived superhydrophilic carbon for supercapacitors. *Green Chem.* **2021**, *23*, 3400–3409. [[CrossRef](#)]
3. Park, H.; May, A.; Portilla, L.; Dietrich, H.; Münch, F.; Rejek, T.; Sarcletti, M.; Banspach, L.; Zahn, D.; Halik, M. Magnetite nanoparticles as efficient materials for removal of glyphosate from water. *Nat. Sustain.* **2020**, *3*, 129–135. [[CrossRef](#)]
4. Reza, M.T.; Rottler, E.; Tolle, R.; Werner, M.; Ramm, P.; Mumme, J. Production, characterization, and biogas application of magnetic hydrochar from cellulose. *Bioresour. Technol.* **2015**, *186*, 34–43. [[CrossRef](#)] [[PubMed](#)]
5. Li, C.; Sun, X.; Zhu, Y.; Liang, W.; Nie, Y.; Shi, W.; Ai, S. Core-shell structural nitrogen-doped carbon foam loaded with nano zero-valent iron for simultaneous remediation of Cd (II) and NAP in water and soil: Kinetics, mechanism, and environmental evaluation. *Sci. Total Environ.* **2022**, *832*, 155091. [[CrossRef](#)]
6. Creamer, A.E.; Gao, B. Carbon-Based Adsorbents for Postcombustion CO<sub>2</sub> Capture: A Critical Review. *Environ. Sci. Technol.* **2016**, *50*, 7276–7289. [[CrossRef](#)]
7. Jin, H.L.; Feng, X.; Li, J.; Li, M.; Xia, Y.Z.; Yuan, Y.F.; Yang, C.; Dai, B.; Lin, Z.Q.; Wang, J.C.; et al. Heteroatom-Doped Porous Carbon Materials with Unprecedented High Volumetric Capacitive Performance. *Angew. Chem. Int. Edit.* **2019**, *58*, 2397–2401. [[CrossRef](#)]

8. Demir, M.; Doguscu, M. Preparation of Porous Carbons Using NaOH, K<sub>2</sub>CO<sub>3</sub>, Na<sub>2</sub>CO<sub>3</sub> and Na<sub>2</sub>S<sub>2</sub>O<sub>3</sub> Activating Agents and Their Supercapacitor Application: A Comparative Study. *ChemistrySelect* **2022**, *7*, e202104295. [[CrossRef](#)]
9. Chen, Z.; Liu, T.; Tang, J.J.; Zheng, Z.J.; Wang, H.M.; Shao, Q.; Chen, G.L.; Li, Z.X.; Chen, Y.Q.; Zhu, J.W.; et al. Characteristics and mechanisms of cadmium adsorption from aqueous solution using lotus seedpod-derived biochar at two pyrolytic temperatures. *Environ. Sci. Pollut. Res.* **2018**, *25*, 11854–11866. [[CrossRef](#)]
10. Zhao, X.C.; Wang, A.Q.; Yan, J.W.; Sun, G.Q.; Sun, L.X.; Zhang, T. Synthesis and Electrochemical Performance of Heteroatom-Incorporated Ordered Mesoporous Carbons. *Chem. Mater.* **2010**, *22*, 5463–5473. [[CrossRef](#)]
11. Zhang, Y.J.; Mori, T.; Ye, J.H.; Antonietti, M. Phosphorus-Doped Carbon Nitride Solid: Enhanced Electrical Conductivity and Photocurrent Generation. *J. Am. Chem. Soc.* **2010**, *132*, 6294–6295. [[CrossRef](#)] [[PubMed](#)]
12. Shen, Z.F.; Liu, C.L.; Yin, C.C.; Kang, S.F.; Liu, Y.A.; Ge, Z.G.; Xia, Q.N.; Wang, Y.G.; Li, X. Facile large-scale synthesis of macroscopic 3D porous graphene-like carbon nanosheets architecture for efficient CO<sub>2</sub> adsorption. *Carbon* **2019**, *145*, 751–756. [[CrossRef](#)]
13. Wang, L.L.; Zhu, D.Q.; Chen, J.W.; Chene, Y.S.; Chen, W. Enhanced adsorption of aromatic chemicals on boron and nitrogen co-doped single-walled carbon nanotubes. *Environ. Sci.-Nano* **2017**, *4*, 558–564. [[CrossRef](#)]
14. Wei, J.H.; Cai, W.Q. One-step hydrothermal preparation of N-doped carbon spheres from peanut hull for efficient removal of Cr(VI). *J. Environ. Chem. Eng.* **2020**, *8*, 104449. [[CrossRef](#)]
15. Saha, D.; Barakat, S.; Van Bramer, S.E.; Nelson, K.A.; Hensley, D.K.; Chen, J.H. Noncompetitive and Competitive Adsorption of Heavy Metals in Sulfur-Functionalized Ordered Mesoporous Carbon. *ACS Appl. Mater. Inter.* **2016**, *8*, 34132–34142. [[CrossRef](#)]
16. Wei, Y.; Xu, L.; Yang, K.; Wang, Y.; Wang, Z.L.; Kong, Y.; Xue, H.G. Electrosorption of Toxic Heavy Metal Ions by Mono S- or N-Doped and S, N-Codoped 3D Graphene Aerogels. *J. Electrochem. Soc.* **2017**, *164*, E17–E22. [[CrossRef](#)]
17. Chen, F.; Zhang, M.; Ma, L.L.; Ren, J.G.; Ma, P.; Li, B.; Wu, N.N.; Song, Z.M.; Huang, L. Nitrogen and sulfur codoped micro-mesoporous carbon sheets derived from natural biomass for synergistic removal of chromium(VI): Adsorption behavior and computing mechanism. *Sci. Total. Environ.* **2020**, *730*, 138930. [[CrossRef](#)]
18. Chen, H.; Yu, F.; Wang, G.; Chen, L.; Dai, B.; Peng, S.L. Nitrogen and Sulfur Self-Doped Activated Carbon Directly Derived from Elm Flower for High-Performance Supercapacitors. *ACS Omega* **2018**, *3*, 4724–4732. [[CrossRef](#)]
19. Sun, Z.J.; Liao, J.H.; Sun, B.; He, M.L.; Pan, X.; Zhu, J.P.; Shi, C.W.; Jiang, Y. Nitrogen Self-Doped Porous Carbon Materials Derived from a New Biomass Source for Highly Stable Supercapacitors. *Int. J. Electrochem. Sci.* **2017**, *12*, 12084–12097. [[CrossRef](#)]
20. Liu, W.J.; Tian, K.; Ling, L.L.; Yu, H.Q.; Jiang, H. Use of Nutrient Rich Hydrophytes to Create N,P-Dually Doped Porous Carbon with Robust Energy Storage Performance. *Environ. Sci. Technol.* **2016**, *50*, 12421–12428. [[CrossRef](#)]
21. Yue, L.M.; Xia, Q.Z.; Wang, L.W.; Wang, L.L.; DaCosta, H.; Yang, J.; Hu, X. CO<sub>2</sub> adsorption at nitrogen-doped carbons prepared by K<sub>2</sub>CO<sub>3</sub> activation of urea-modified coconut shell. *J. Colloid Interf. Sci.* **2018**, *511*, 259–267. [[CrossRef](#)] [[PubMed](#)]
22. Zhu, Y.Y.; Chen, M.M.; Zhang, Y.; Zhao, W.X.; Wang, C.Y. A biomass-derived nitrogen-doped porous carbon for high-energy supercapacitor. *Carbon* **2018**, *140*, 404–412. [[CrossRef](#)]
23. Fuertes, A.B.; Sevilla, M. Superior Capacitive Performance of Hydrochar-Based Porous Carbons in Aqueous Electrolytes. *Chemsuschem* **2015**, *8*, 1049–1057. [[CrossRef](#)] [[PubMed](#)]
24. Sevilla, M.; Ferrero, G.A.; Fuertes, A.B. Beyond KOH activation for the synthesis of superactivated carbons from hydrochar. *Carbon* **2017**, *114*, 50–58. [[CrossRef](#)]
25. Tang, F.Y.; Wang, L.Q.; Liu, Y.N. Biomass-derived N-doped porous carbon: An efficient metal-free catalyst for methylation of amines with CO<sub>2</sub>. *Green Chem.* **2019**, *21*, 6252–6257. [[CrossRef](#)]
26. Tsubouchi, N.; Nishio, M.; Mochizuki, Y. Role of nitrogen in pore development in activated carbon prepared by potassium carbonate activation of lignin. *Appl. Surf. Sci.* **2016**, *371*, 301–306. [[CrossRef](#)]
27. Luo, J.W.; Jia, C.; Shen, M.H.; Zhang, S.C.; Zhu, X.D. Enhancement of adsorption and energy storage capacity of biomass-based N-doped porous carbon via cyclic carbothermal reduction triggered by nitrogen dopants. *Carbon* **2019**, *155*, 403–409. [[CrossRef](#)]
28. Jia, C.; Yu, F.; Luo, J.; Chen, C.; Zhang, S.; Zhu, X. Three birds with one stone approach to superior N/S co-doped microporous carbon for gas storage and water purification. *Chem. Eng. J.* **2021**, *431*, 133231. [[CrossRef](#)]
29. Xu, L.; Wu, C.X.; Liu, P.H.; Bai, X.; Du, X.Y.; Jin, P.K.; Yang, L.; Jin, X.; Shi, X.; Wang, Y. Peroxymonosulfate activation by nitrogen-doped biochar from sawdust for the efficient degradation of organic pollutants. *Chem. Eng. J.* **2020**, *387*, 124065. [[CrossRef](#)]
30. Ma, L.J.; Wang, Q.; Islam, S.M.; Liu, Y.C.; Ma, S.L.; Kanatzidis, M.G. Highly Selective and Efficient Removal of Heavy Metals by Layered Double Hydroxide Intercalated with the MoS<sub>4</sub><sup>2-</sup> Ion. *J. Am. Chem. Soc.* **2016**, *138*, 2858–2866. [[CrossRef](#)]
31. Zhu, X.D.; Liu, Y.C.; Luo, G.; Qian, F.; Zhang, S.C.; Chen, J.M. Facile Fabrication of Magnetic Carbon Composites from Hydrochar via Simultaneous Activation and Magnetization for Triclosan Adsorption. *Environ. Sci. Technol.* **2014**, *48*, 5840–5848. [[CrossRef](#)] [[PubMed](#)]
32. Zhu, X.D.; Liu, Y.C.; Zhou, C.; Zhang, S.C.; Chen, J.M. Novel and High-Performance Magnetic Carbon Composite Prepared from Waste Hydrochar for Dye Removal. *ACS Sustain. Chem. Eng.* **2014**, *2*, 969–977. [[CrossRef](#)]
33. Sevilla, M.; Ferrero, G.A.; Diez, N.; Fuertes, A.B. One-step synthesis of ultra-high surface area nanoporous carbons and their application for electrochemical energy storage. *Carbon* **2018**, *131*, 193–200. [[CrossRef](#)]
34. Muttakin, M.; Mitra, S.; Thu, K.; Ito, K.; Saha, B.B. Theoretical framework to evaluate minimum desorption temperature for IUPAC classified adsorption isotherms. *Int. J. Heat Mass Tran.* **2018**, *122*, 795–805. [[CrossRef](#)]

35. Chen, H.; Zhou, M.; Wang, Z.; Zhao, S.Y.; Guan, S.Y. Rich nitrogen-doped ordered mesoporous phenolic resin-based carbon for supercapacitors. *Electrochim. Acta* **2014**, *148*, 187–194. [[CrossRef](#)]
36. Din, A.T.M.; Ahmad, M.A.; Hameed, B.H. Ordered mesoporous carbons originated from non-edible polyethylene glycol 400 (PEG-400) for chloramphenicol antibiotic recovery from liquid phase. *Chem. Eng. J.* **2015**, *260*, 730–739. [[CrossRef](#)]
37. Yang, J.; Ji, G.; Gao, Y.; Fu, W.; Irfan, M.; Mu, L.; Zhang, Y.; Li, A. High-yield and high-performance porous biochar produced from pyrolysis of peanut shell with low-dose ammonium polyphosphate for chloramphenicol adsorption. *J. Clean. Prod.* **2020**, *264*, 121516. [[CrossRef](#)]
38. Chen, A.; Pang, J.; Wei, X.; Chen, B.; Xie, Y. Fast one-step preparation of porous carbon with hierarchical oxygen-enriched structure from waste lignin for chloramphenicol removal. *Environ. Sci. Pollut. Res. Int.* **2021**, *28*, 27398–27410. [[CrossRef](#)] [[PubMed](#)]